Universidad Carlos III de Madrid
e-Archivo

Institutional Repository

This document is published in:

Chemical Engineering Journal (2013). 230, 573-583.
DOI: http://dx.doi.org/10.1016/j.cej.2013.06.112

© 2013 Elsevier B.V.

NOTICE: this is the author's version of a work that was accepted for publication in Chemical Engineering Journal. Changes resulting from the publishing process, such as peer review, editing, corrections, structural formatting, and other quality control mechanisms may not be reflected in this document. Changes may have been made to this work since it was submitted for publication. A definitive version was subsequently published in Chemical Engineering Journal 230 (2015) pp. 573-583. doi:10.1016/j.cej.2013.06.112

Thermal energy storage in a fluidized bed of PCM

M.A. Izquierdo-Barrientos[a,*], C. Sobrino[a], J.A. Almendros-Ibáñez[b,c]

[a] *Universidad Carlos III de Madrid, ISE Research Group, Thermal and Fluid Engineering Department, Avda. de la Universidad 30, 28911 Leganés, Madrid, Spain*
[b] *Escuela de Ingenieros Industriales, Dpto. de Mecánica Aplicada e Ingeniería de Proyectos, Castilla La Mancha University, Campus universitario s/n, 02071, Albacete, Spain*
[c] *Renewable Energy Research Institute, Section of Solar and Energy Efficiency, C/ de la Investigación s/n, 02071, Albacete, Spain*

Abstract

The objective of the present work was to research the storage behavior of a fluidized bed filled with a granular phase change material (PCM) with a small particle diameter ($\overline{d_p} = 0.54$ mm). The performance of the fluidized bed was compared to that of well-known storage methods such as fluidized beds with sand and packed beds based of sand and PCM. For this purpose, heating experiments were conducted in a cylindrical bed with air as the working fluid.

The influence of the bed height and flow rate on the storage and recovery efficiencies of the fluidized bed of PCM was analyzed. Additionally, the stability of the PCM during various charging-discharging cycles was studied.

The results indicate that this PCM is an alternative material that can be used in fluidized bed systems to increase the efficiency of storing thermal

*Corresponding author. Tel.:+34 91 624 83 71
Email address: maizquie@ing.uc3m.es (M.A. Izquierdo-Barrientos)

energy in the form of latent heat. Under the experimental conditions tested in this study, higher charging efficiencies were observed for fixed and fluidized beds based on PCM than those of sand. High gas velocity and low bed height shorten the charging time but also reduce the charging efficiency. The cycling test shows that the PCM is stable under bubbling conditions up to 15 cycles, which corresponds to approximately 75 hours of continuous operation.

Keywords:
Fluidization, Packed bed, Phase change, Heat transfer, Energy,
Thermodynamics process

---

1. Introduction

Energy storage is needed in many applications when the availability and demand for energy do not coincide. Sensible heat storage is the most common method of thermal energy storage, although research on advanced materials and systems for latent thermal storage has increased recently because the density of stored energy is greater for latent thermal storage than for sensible heat storage. Additional information about Phase Change Materials (PCM), their classification and applications in thermal storage can be found in different reviews [1, 2, 3].

Packed beds are a suitable option when air is used as the heat transfer fluid. Moreover, micro-encapsulation of phase change materials has been proposed as a heat transfer enhancement technique for latent heat thermal storage because it increases the heat transfer area. Similar to packed beds, fluidized beds can be utilized for thermal energy storage and have some properties, such as a uniform temperature in the bed or a high rate of heat

transfer to a solid object within the bed, which can be advantageous in several applications.

In most cases where published numerical studies have been verified experimentally, the experimental results for packed bed sensible heat storage have been limited to beds of spheres or cylinders with large characteristic diameters on the order of 1 cm [4]. An experimentally validated heat transfer model for energy storage fixed bed systems [5] shows higher storage efficiencies for smaller particle sizes.

The application of fluidized beds to sensible heat storage has been studied in the past, and it has been shown that a fluidized bed behaves similarly to a well-mixed tank with negligible variations in the temperature along the bed [6]. Wagialla et al. [7] modelled the behavior of a fluidized bed and showed that the optimum performance of the fluidized bed, when it was used as an energy storage device, was achieved by employing a superficial air velocity similar to the minimum fluidization velocity. Moreover, there is an optimum bed height that maximizes the efficiency of energy recovery because the bed height has opposite effects on the residence time and the heat transfer coefficient.

Packed beds for latent thermal energy storage have been studied previously, mainly in beds of macro-encapsulated spheres of PCM with diameters of a few centimeters and water as the heat transfer fluid [8]. The behavior of a packed bed of spherical capsules with a radius of 20-60 mm and filled with a PCM, suitable for use with a solar water heating system, was simulated by Regin et al. [9], who observed that the charging and discharging rates were

significantly higher for capsules of smaller radius than those of larger radius. The transient response of a cylindrical packed bed of PCM encapsulated in 31.8-mm spheres with air as the working fluid was investigated by Benmansour et al. [10], who conducted two-dimensional numerical calculations for the separate phases that were verified by measurement of the temperature of the fluid and the PCM.

In recent years, granular phase changing composites with a small particle diameter (1-3 mm) have been tested in latent heat thermal storage packed bed systems. The utilization of encapsulated phase change materials with a small particle diameter is advantageous in terms of heat transfer rates and pumping requirements when 1) storage systems of small characteristic length are applicable [11], and 2) the time required for the phase change is inversely proportional to the superficial gas velocity and depends on the air supply temperature [12]. A PCM encapsulated in spheres with a diameter of 25 mm and agitated in a liquid-fluidized bed has been tested by Sozen et al. [13], who demonstrated improvements over fixed bed thermal energy storage systems and enhanced the performance of the system by increasing the superficial water velocity. Merry and Rubinsky [14] studied the heat transfer coefficients for a surface immersed in a two-dimensional fluidized bed of solid-to-solid phase transition material particles with a mean diameter of 0.4 mm that were fluidized with air. Heat transfer coefficients were also studied by Brown et al. [15] in a cylindrical gas-fluidized bed containing several types of micro-encapsulated phase change materials undergoing solid-liquid transitions, with nominal diameters ranging from 140 to 655 μm.

The aim of this study was to evaluate the performance of an air-fluidized

bed of micro-encapsulated PCM with a mean diameter of 0.54 mm as a storage system in terms of its charging and discharging efficiencies and stability under continuous operation. The behaviors of a fixed bed of sand, a fluidized bed of sand and a fixed bed of PCM were also studied and compared.

2. Experimental apparatus and materials

In the present study, heating experiments were conducted with sand and PCM in a packed bed and in a fluidized bed. A schematic diagram of the experimental apparatus is illustrated in Figure 1. The bed consists of a cylindrical tube of stainless steel with walls 2 mm thick and filled with particles. The air enters the plenum of the column and then flows into the bed through a distribution plate with a thickness of 1.5 mm containing 300 perforations with a diameter of 2 mm, which results in a 3% open area. In this way, the air is uniformly distributed in the bed. A fine mesh screen is mounted at the bottom of the distributor plate to prevent the solid particles from entering the plenum chamber. The instrumentally monitored section of the test apparatus has a height of 500 mm and an internal diameter of 200 mm, and it is insulated with glass wool with a thickness of 2 cm. Additionally, the piping is insulated with a thermal insulator with a thickness of 1 cm. The free board of the column is divided into two parts: 1) a cylinder with an internal diameter of 200 mm, and 2) another cylinder with an internal diameter of 300 mm. The purpose of these two parts is to assure the homogeneous velocity distribution of air at the exit from the test section and to reduce the elutriation and entrainment of particles from the bed.

[Figure 1 about here.]

The air flow is produced by a blower with variable mass flow rate, and heated by electrical heaters before flowing into the column. Type K thermocouples are used to measure the temperature at specific locations inside the test section and in the plenum chamber. At these locations, pressure variations can be measured using pressure sensors with two different ranges: 100 mbar and 1 bar. Air temperatures are also measured at the inlet and outlet of the test section. The thermocouples and pressure sensors are connected to a data acquisition system for continuous monitoring and recording of the data.

The materials used for the experiments are sand, which is a typical material used in fixed and fluidized beds, and a granular phase changing composite (Rubitherm®-GR50). The material that changes its phase is paraffin, and it is bound within a secondary supporting structure of SiO_2 . This composite material is commercially available in two sizes: a coarser grade with a particle size between 1 and 3 mm, which is suitable for use in a fixed bed Rady [11, 16], and a finer grade with a particle size between 0.2 and 0.6 mm. The sand and the finer GR50 material correspond to group B according to Geldart's classification [17], which means that the sand and the finer GR50 composite fluidize easily with vigorous bubbling action and that bubbles grow large [18]. In addition, the use of two different PCM particle sizes permits the use of the same gas flow rate (450 l/min) in the fixed bed configuration for the sand and the coarser PCM, and also a similar excess gas velocity over minimum fluidization conditions $U/U_{mf} \approx 1.7$ in the fluidized bed for the sand and the finer PCM.

Some properties of the sand and PCM such as density (ρ), thermal conductivity (k) and mean diameter of the particles $\overline{d_p}$ (with its standard deviation , σ_{dp}) are shown in Table 1. In addition, the variation of the specific heat with temperature is presented for each material in Figure 2. For the GR50 composite, the variation of specific heat with temperature is nearly the same for the two grades, and, therefore, only one case is shown. For the PCM, the curve of the specific heat versus temperature shows a clear peak between 42 and 50°C where the phase change process occurs. In solid form there is small variation of the specific heat around 30°C, which corresponds with a solid-solid transition. Under 20°C the specific heat is approximately constant around $1.45\,kJ/(kg \cdot K)$. In contrast, the curve for sand is approximately linear, varying between $0.6kJ/(kg{\cdot}K)$ for 20°C and $0.8kJ/(kg{\cdot}K)$ for 95°C.

[Table 1 about here.]

[Figure 2 about here.]

Differential scanning calorimetry (DSC) is the technique used to study the specific heat variation for the sand and the PCM. The tests were carried out using a sapphire standard. For the coarser PCM one granule was placed in the DSC sample pan while for the finer PCM and the sand a handful of granules was used. A heating rate of 0.5 °C/min was selected. According to Rady [16], who studied in detail the same granular PCM used in our work, this heating rate is slow enough to guarantee that the onset of crystallization occurs at the same temperature as the termination of the melting process. This DSC method has also been used to study the phase

changing behavior of the granular GR50. The characterization results are shown in Table 2. These DSC results include the specific heats of the solid and liquid phases ($c_{p,s}, c_{p,l}$), the latent heat of phase change (h_{ls}) and the characteristic temperatures of the phase change: T_{on} (onset temperature), T_{end} (endset temperature), T_s (extrapolated starting temperature), T_e (extrapolated ending temperature) and T_p (peak temperature)[16].

[Table 2 about here.]

For the comparison between fixed and fluidized beds of sand and PCM, a static bed height of $H = 200\,mm$ is defined for all of the experiments in order to have the same storage volume in all cases. The column is filled with $5\,kg$ of PCM or $9\,kg$ of sand. When we analyze the influence of flow rate on the operation of the fluidized bed of PCM, the height of the bed is fixed at $200\,mm$ and the flow rate is varied. For the study of the influence of the bed height on the performance of the bed, the flow rate remains constant while the bed height is augmented and the mass of solids in the bed varies accordingly.

The bed temperature is uniform and equal to the ambient temperature at the beginning of every experiment. An experiment starts by blowing air at the desired rate into the column and switching on the electric heaters with the required power. The air is heated from room temperature up to $65°C$ by regulating the electrical resistance power using a PID controller with the control thermocouple placed at the plenum chamber. The PID controller has been selected to provide the same supply temperature pattern for all of the experiments.

When the temperature along the bed is stabilized, the blowing air is no longer heated. Then, the inlet temperature of the air and the bed temperature both start to decrease. Temperatures are measured on the bed axis at different heights from the distributor: 25, 75, 125, 175 and 425 mm, where the last location (425 mm) is above the bed surface.

2.1. Hydrodynamics of the fluidized bed

Figure 3 shows the distributor pressure drop Δp_{dist} for different superficial gas velocities, $U(m/s)$. These data can be properly fit to a parabola shape.

[Figure 3 about here.]

The pressure drop across the bed of particles, Δp_{bed}, is defined as the distributor pressure drop subtracted from the pressure drop of the system when it is filled with particles [19]. Thus,

$$\Delta p_{bed} = \Delta p_{system} - \Delta p_{dist} \tag{1}$$

The pressure drop of the system, Δp_{system}, is the pressure difference between the plenum chamber and the ambient pressure measured when the bed is filled (to a height equal to the bed diameter) with sand and the finer grade of GR50. Figure 4 shows the pressure across the bed as function of the superficial gas velocity for the sand and for the finer grade of GR50. These measurements are used to determine the minimum fluidization velocity of each material, U_{mf}. The minimum fluidization velocity is usually

defined as the intersection of the horizontal fluidized bed line and the sloping packed bed line, [20], which results in $U_{mf} = 0.33m/s$ for the sand and $U_{mf} = 0.13m/s$ for the finer GR50 grade.

[Figure 4 about here.]

The flow rates for the fluidization experiments are chosen to provide the same excess air, U/U_{mf}, conditions for the different experiments. Therefore, the flow rates are 450 l/min for both fixed beds, and 450 l/min and 1,000 l/min for the fluidized beds of the PCM material and the sand, respectively (because the PCM and sand have different minimum fluidization velocities.) At these flow rates, both fluidized materials are working with an excess of air velocity over the minimum fluidization conditions, U/U_{mf}, of approximately 1.7. The fixed bed height is the same in the two cases so both fluidization experiments are comparable because they are under similar bubbling conditions.

3. Results and discussion

Four experiments are performed to compare the behavior of a bed filled with PCM and that of a bed filled with sand. Figure 5 shows the temperatures that are measured at different heights during the charging and discharging processes for the four different configurations.

[Figure 5 about here.]

Under fluidization conditions, the temperature along the bed is uniform regardless of the fluidized material (either sand or PCM) because the system behaves similarly to a well mixed tank [18]. Three of the four thermocouples inside the bed (the thermocouples located at 7.5, 12.5 and 17.5 cm above the distributor) measure the same temperature during the charging process. The first thermocouple, located only 2.5 cm over the distributor, shows a higher temperature than the other thermocouples during almost the whole process. These results could be attributed to the influence of the air jets from the distributor perforations [21]. These jets could be long enough to modify the temperature measured by the first thermocouple. The temperature measured at 2.5 cm is thus an average of the air temperature coming from the plenum chamber through the distributor and the bed temperature.

For fixed bed conditions, the behavior is different. The bed behaves similarly to a plug flow system. The regions of the bed closer to the distributor are heated before those regions located farther away from the distributor. In the tests with GR50, this composite material takes longer than sand to reach the set temperature because of the latent heat that is stored while the phase change is taking place around $50°C$.

For the fixed bed experiments, the phase change takes place at different times at different heights because of the temperature stratification, in accordance with results presented by Rady [11]. In contrast, in the fluidized bed, the phase change of the material takes place uniformly throughout the whole bed.

To analyze the experiments, two parameters were studied: the storage efficiency during the charging process, η_C, and the recovery efficiency of the discharging process, η_R [6, 22].

The storage efficiency is defined as follows:

$$\eta_C = \frac{E_s}{E_{in}} = \frac{\rho_s(1-\varepsilon)A_t \int_{x=0}^{x=H} (i_{b_x} - i_0)\, dx}{\int_{t=0}^{t} \dot{m}_{air}\, c_{p,air}\, (T_{air} - T_0)\, dt} \tag{2}$$

where ρ_s is the solid density (sand or PCM), ε the voidage of the bed, $A_t = (\pi/4)\, D^2$ the cross section of the bed, $\dot{m}_{air}$ is the mass flow rate of air to the bed, $c_{p,air}$ is the specific heat of the air as a function of T_{air} (inlet air temperature), T_0 is the initial bed temperature and $i_{b_x} - i_0$ is the specific energy stored in the bed defined in Equation 3.

$$i_{b_x} - i_0 = \int_{T_0}^{T_{b_x}} c_p\, dT \tag{3}$$

where c_p is the apparent specific heat of the material in the bed as a function of T_{b_x} (the bed temperature at height x and time t).

According to Equation (2) η_C relates the energy stored, E_s, in the bed at time t and the total thermal energy supplied by the air at the inlet of the bed, E_{in}, (relative to the initial temperature of the bed T_0) up to the same time, t. The value of the energy stored in the bed at a given time has been calculated by dividing the bed into four elements because there are four thermocouples in the bed (at heights x = 2.5, 7.5, 12.5 and 17.5 cm).

[Figure 6 about here.]

The variation of η_C with time for the sand and the GR50 PCM in the fixed bed is presented in Figure 6(a) and that for the same materials under fluidized conditions is presented in Figure 6(b). The efficiency is higher with the GR50 material than with the sand for both types of beds. This is due to the inherent characteristics of both materials. One of the main advantages of the PCM is its high capacity of storing energy per unit volume. In this case, the energy storage capacity of the GR50 is approximately double of the energy capacity of the sand in the same volume. Therefore, when the temperature reaches the maximum and steady temperature (after approximately two hours) the maximum efficiency of the GR50 for the fixed bed is twice the maximum efficiency of the sand (see Figure 6(a)). Another advantage of the GR50 over the sand is its lower density and minor particle size, which permits to fluidize the GR50 PCM with a lower air flow rate. In the experiments compared in Figure 6(b) the air flow rate in the GR50 PCM is approximately half of the flow rate used with the sand. As a consequence, the maximum efficiency of the GR50 is approximately four times higher than the maximum efficiency of the sand when the temperature of the bed reaches the maximum and steady temperature.

The first minutes of each experiment should not be taken into account as they correspond to the stabilization of the system. After this stabilization period, the efficiency increases with the bed temperature because the inlet air is also being heated during the charging process. When the inlet air temperature reaches its maximum achievable value, the efficiency starts to decrease. The variation of the efficiency for the sand is smooth in both fixed and fluidized conditions. In contrast, the curves obtained for the PCM show abrupt changes in slope at the beginning and end of the phase change

process. In the fixed bed (Figure 6(a)) appear four changes in the slope of the curve, which correspond with the phase change process detected by each one of the four thermocouples in the bed. The highest efficiency for the fixed bed case is found to occur when the thermocouple placed at 7.5 cm detects the phase change. Under fluidized conditions (Figure 6(b)), only one change in the slope is observed between 0.5 and 1.0 hours, because it is well mixed and the phase change transition occurs homogenously in the bed.

When the temperature in the bed is stabilized, the electric heaters stop heating the air and the blowing air continues to flow at the same rate as the original heated flow. To analyze this discharging process, the recovery efficiency, η_R, is defined as follows [6],

$$\eta_R = \frac{E_d}{E_{d,max}} = \frac{\rho_s(1-\varepsilon)A_t \int_{x=0}^{x=H} (i_{b_{max}} - i_x)\, dx}{\rho_s(1-\varepsilon)A_t \int_{x=0}^{x=H} (i_{max} - i_{end})\, dx} = \frac{\int_{x=0}^{x=H} \int_{T_{b_x}}^{T_{b_{max}}} c_p\, dT\, dx}{\int_{x=0}^{x=H} \int_{T_{end}}^{T_{max}} c_p\, dT\, dx} \tag{4}$$

where E_d names the energy obtained during the discharging period up to the time t, $E_{d,max}$ represents the maximum available energy at the discharge, T_{b_x} is the bed temperature at height x and time t, $T_{b_{max}}$ is the maximum bed temperature achieved at the end of the charging process, T_{max} corresponds to the supply air temperature at steady state conditions and T_{end} is the temperature of the bed at the end of the experiment.

Figures 7(a) and 7(b) represent the evolution of the recovery efficiency for the fixed and fluidized beds with sand and PCM, respectively.

The bed temperature for the four experiments does not decrease to the initial temperature because the supplied air is heated by the blower, thereby achieving a higher temperature than the ambient temperature. The difference between the T_{end} and the room temperature depends on the flow rate. Thus, for the fluidized bed with sand, this difference is maximized when the flow rate is highest.

[Figure 7 about here.]

The recovery efficiency for the fixed beds (Figure 7(a)) shows better behavior for sand than GR50 during the first hour because of the time required for the solidification of the PCM. Thus, the 'steps' in the PCM curve correspond to the phase change. Nevertheless, after the first hour, the efficiency parameter is the same for both materials.

For the recovery efficiency in fluidized beds (Figure 7(b)), the efficiency during the first hour is higher for sand than for GR50, as also observed for the fixed beds. In contrast, when the recovery efficiency is stabilized in both fluidized beds, the PCM presents higher efficiency (0.94) than sand (0.89).

3.1. Influence of flow rate

To study the influence of flow rate on the performance of the fluidized bed with PCM, four different cases were studied. In all of these experiments, the mass of PCM was 5 kg and the air flow was heated from room temperature up to 65°C. The flow rates selected were 625, 500, 450 and 375 l/min,

which correspond to an excess air velocity over the minimum fluidization conditions, U/U_{mf}, of 2.5, 2, 1.7 and 1.5, respectively.

In Figure 8, the temperature distributions along the bed for the four experiments are presented. The temperatures plotted in this figure are the control temperature; the temperature measured by the first thermocouple, which was located 2.5 cm from the distributor; the mean temperature in the bed, which was calculated from data obtained by the other three thermocouples at 7.5, 12.5 and 17.5 cm; and the temperature of the air at the outlet section. The influence of the air jets on the temperature of the first thermocouple is also observed in the four cases shown in Figure 8.

[Figure 8 about here.]

Before proceeding to the analysis of these experimental results, it is convenient to introduce the following dimensionless bed average temperature:

$$\overline{\theta}_b = \frac{\overline{T}_b - T_0}{T_{max} - T_0} \tag{5}$$

where $\overline{T}_b$ is the average temperature of the bed, T_0 is the initial temperature of the bed and T_{max} is the supplied air temperature at steady state conditions (in this case, $65°C$.)

To analyze these experiments, η_C and η_R were calculated. In Figure 9(b), the efficiency during the charging process for the four experiments is shown. Furthermore, for better understanding, the dimensionless tempera-

ture for each charging test is presented in Figure 9(a).

The results of the efficiency evolution show that, disregarding the stabilization period, higher values of efficiency are reached once the supply air temperature attains its maximum difference with respect to the bed temperature. When the maximum steady temperature is reached in the bed, after approximately two hours of operation, the higher the air flow rate the lower the discharge efficiency because E_{in} increases for the same stored energy (see Equation (2)). However, a higher flow rate permits the set temperature to be achieved more quickly.

[Figure 9 about here.]

The dimensionless temperature and evolution efficiency during the recovery process are shown in Figure 10. The dimensionless temperature for the discharging process when $U/U_{mf} = 2.5$ (Figure 10(a)) shows that no phase change occurs because the blower heats the air flow above the phase change temperature. Thus, the recovery efficiency is not plotted for this case in Figure 10(b).

Regarding the charging process, similar efficiencies are observed at the end of the recovery process for the different flow rates, and the phase change occurs sooner at a higher flow rate.

[Figure 10 about here.]

3.2. Influence of bed height

The influence of the bed height in the fluidized bed filled with PCM is investigated. Three experiments were performed at various bed heights. The air is heated from room temperature up to $65°C$, and the flow rate selected (500 l/min) is the same for all experiments. The three chosen heights are 100, 200 and 300 mm, which correspond to 0.5, 1 and 1.5 times the diameter of the bed, respectively. In Figure 11, the temperature distributions along the bed for the three experiments are presented.

[Figure 11 about here.]

The dimensionless temperature and efficiency for the charging process are presented in Figure 12. The time required to achieve a certain temperature is longer when the mass of the material is higher because the input energy is the same for the three different cases. However, increased charging efficiency is obtained when the mass is higher (see Figure 12(b)) as there is more material available to store heat while the input energy is the same. When the bed reaches a steady state, the maximum temperature attained decreases as the bed height increases, possibly because of small thermal losses to the ambient surroundings, although the bed is insulated. When the bed height is doubled (or tripled), the heat transfer area for heat losses is also doubled (or tripled), thereby increasing the thermal losses. For the bed height of 0.5D, the bed temperature undergoes fluctuations that may be caused by the proximity of the thermocouple to the freeboard, where the bursting bubbles may affect the measurements.

[Figure 12 about here.]

In Figure 13, the dimensionless temperature and evolution efficiency during the recovery process are shown. Figure 13(a) shows that it takes more time to discharge the bed when the mass is higher, and better recovery efficiency coefficients are obtained when less mass is introduced (see Figure 13(b)). This last effect is a result of the higher thermal losses to the ambient surroundings from the larger beds, which results in a lower bed temperature at the beginning of the recovery process. Therefore, less of the energy supplied by the inlet gas during the charging process is recovered by the system.

[Figure 13 about here.]

3.3. Cycling behavior

Micro-encapsulated PCM may be prone to fracture and cracking because of collisions and shearing when fluidized by air. There are different studies in the literature concerning the stability of micro-PCMs in slurries [23, 24, 25] and they conclude that rupture of the micro-capsules in slurries is reduced diminishing the particle size and increasing the thickness of the encapsulation. Nevertheless, the different phenomena that influence on the stability of micro-PCM slurries are different to those appearing in a bubbling fluidized bed and a direct comparison is not possible. The micro-PCMs used typically in slurries have a size around or under 10 μm whereas we are using particles of $\overline{d_p} = 0.54$ mm. Also the particle concentration in slurries is usually much lower than in fluidized beds, which is around 60%.

In fluidized beds the attrition is the phenomenon responsable for particle fragmentation. Two different attrition mechanisms can be observed [26]:

abrasion and fragmentation. In the first, particles of much smaller size are removed from the particle surface. As a result, the particle size distribution is slightly modified although the percentage of fines is increased. The final size distribution is bimodal. In the second mechanism, the original particles break into particles of similar size. The particle size distribution is notably broader with a distinctly smaller mean particle size. Ray et al. [27] and Pis et al. [28] concluded that the dominant mechanism in most fluidized bed applications is abrasion.

To study the cycling behavior and the attrition of the PCM, 15 heating and cooling cycles were conducted under the same conditions ($U = 500l/min$, GR50 heated up to 65°C). Samples of 250 g of GR50 were extracted from the bed after certain cycles to study the particle size evolution. Some of the cycling curves are presented in Figure 14. The uniformity of the temperature in the bed measured during thermal cycling indicates that the fluidization quality of the phase change material used in this study is not affected by the number of cycles and that the cycling stability is ensured. No loss of heat storage or recovery capacity during thermal cycling appears. Furthermore, the set temperature (65°C) is achieved sooner in the sequence of cycles. One reason could be the small differences between the size distributions in the sequence of cycles. When the number of cycles is increased, the particles become smaller, the heat transfer area increases, and, hence, the heat transfer improves.

The particle size distributions after each cycle have been determined by sieve analysis. Figure 15 represents the cumulative distribution function showing the weight percent of particles passing through a sieve of a given aperture between the initial distribution and the end of two different cycles. The variation observed in the particle size distribution indicates that abra-

sion is present in the fluidized bed with GR50. The mean particle size is slightly reduced, the external surface of the particles is eroded increasing the content of fines in the bed but the PCM remains encapsulated. In Figure 15 it can be seen that the percentage of fines is not augmented because no cyclone or dispositive has been used to collect them, so they are probably lost during the fluidized bed operation. The rate of erosion reduces with time because the rugosities of the particles are filed and the surface is smoothed. Only if the thickness of the encapsulation is not large enough the abrasion could provoke the lost of PCM. If the PCM leaks out when it is in liquid form it can stick a group of particles, forming agglomerates similar to the ones observed by other researchers in slurries [24]. If this happens the bed would be probably defluidized because the air flow rate could not fluidize particles of such size, but this problem is not observed in our work. If the PCM studied in this work is going to be used in an actual process, probably the material will suffer more than 15 cycles. For a specific application, the PCM should be previously tested under the same charging-discharging times and temperatures of the application, which could be different from the ones used in this work. The number of cycles that the PCM keeps its properties must be large enough to be economically profitable in comparison with a conventional storage facility. Nevertheless, this number of cycles strongly depends on the application and has to be studied for each particular case.

[Figure 14 about here.]

[Figure 15 about here.]

4. Conclusions

In this paper, the performance of an air-fluidized bed of micro-encapsulated PCM as a thermal storage system was studied. Its performance was compared to that of other storage methods: a fluidized bed of sand and fixed beds with sand and PCM. It is concluded that the PCM is an alternative material that can be used to increase the efficiency of storing thermal energy in the form of latent heat in fluidized bed systems.

Under the experimental conditions tested in this work, greater charging efficiencies are observed for the PCM than sand in fixed and fluidized beds. Furthermore, when the charging efficiency is stabilized, the PCM shows similar results for both beds. The PCM also presents better recovery efficiency for both beds after the solidification time.

The study of the influence of the bed height showed that it takes longer to achieve a certain temperature when more mass is used, but higher efficiency values are obtained. The analysis of the influence of the flow rate showed that a higher the flow rate permits the set temperature to be achieved more quickly. At the end of the charging process, similar efficiencies are measured at the different flow rates studied. The cycling study reveals that the PCM suffers attrition during the fluidization process, although no loss of PCM is observed under the experimental conditions tested in this work (75 hours of continuous operation with 15 charging-discharging cycles).

Acknowledgments

This work was founded partially by the Spanish Government (Project

ENE2010-15403), the regional Government of Castilla-La Mancha (Project PPIC10-0055-4054) and Castilla-La Mancha University (Project GE20101662).

5. Notation

A_t Cross section of the bed [m^2]

c_p Specific heat[J/kgK]

$\overline{d_p}$ Mean particle diameter [mm]

D Diameter of the bed [mm]

E Energy [J]

H Height of the bed [mm]

h_{ls} PCM latent heat of fusion [J/kg]

i Specific energy stored in the bed [J/kg]

k Thermal conductivity [W/mK]

m Mass [kg]

$\dot{m}$ Mass flow rate [kg/s]

T Temperature [$^{\circ}C$]

t Time [s]

U Superficial gas velocity $[m/s]$

U_{mf} Minimum fluidization velocity $[m/s]$

5.1. Greek symbols

ρ Density$[kg/m^3]$

σ_{dp} Standard deviation of the mean particle diameter [mm]

Δp Pressure drop [Pa]

$\overline{\theta}$ Dimensionless temperature

η Efficiency

ε Voidage of the bed

5.2. Subscripts

0 Initial

b Bed

C Charging

D Discharging

end End of the discharging process

in Inlet

l Liquid phase

s Solid phase

max Maximum value

x At a specific bed height

6. References

References

[1] B. Zalba, J.M. Marín, L.F. Cabeza, H. Mehling, Review on thermal energy storage with phase change: materials, heat transfer analysis and applications, Appl. Therm. Eng. 23 (2003) 251-283.

[2] L.F. Cabeza, A. Castell, C. Barreneche, A. de Gracia, A.I. Fernández, Materials used as PCM in thermal energy storage in buildings: A review, Renew. Sust. Energ. Rev. 15 (2011) 1675-1695.

[3] A.F. Regin, S.C. Solanki, J.S. Saini, Heat transfer characteristics of thermal energy storage system using PCM capsules: A review, Renew. Sust. Energ. Rev. 12 (2008) 2438-2458.

[4] D. Beasley, J. Clark, Transient response of a packed bed for thermal energy storage, Int. J. Heat Mass Transf. 27 (1984).

[5] M. Hänchen, S. Brückner, A. Steinfeld, High temperature thermal storage using a packed bed of rocks, heat transfer analysis and experimental validation, Appl. Therm. Eng. 31 (2011).

[6] M. Elsayed, I. Megahed, El-Refaee, Experimental testing of fluidized bed thermal storage, Sol. Wind Technol. 5 (1988) 15-25.

[7] K. Wagialla, A. Fakeeha, S. Elnashaire, A. Almaktary, Modeling and simulation of energy storage in fluidized beds using the two-phase model, Energy Sources 13 (1991) 189-201.

[8] L. Xia, P. Zhang, R. Wang, Numerical heat transfer analysis of the packed bed latent heat storage system based on an effective packed bed model, Energy 35-5 (2010) 2022-2032.

[9] A. Regin, S. Solanki, J. Saini, An analysis of a packed bed latent heat thermal energy storage system using pcm capsules: Numerical investigation, Renew. Energy 34 (2009) 1765-1773.

[10] A. Benmansour, M. Hamdan, A. Bengeuddach, Experimental and numerical investigations of solid particles thermal energy storage unit, Appl. Therm. Eng. 26 (2006) 513-518.

[11] M. Rady, Granular phase change materials for thermal energy storage: experiments and numerical simulations, Appl. Therm. Eng. 29 (2009) 3149-3159.

[12] K. Nagano, S. Takeda, T. Mochida, K. Shimakura, Thermal characteristics of a direct heat exchange system between granules with phase change material and air, Appl. Therm. Eng. 24 (2004) 2131-2144.

[13] Z. Sozen, J. Grace, K. Pinder, Thermal energy storage by agitated capsules of phase change material. 1. pilot scale experiments. Ind. Eng. Chem. Res. 27 (1988) 679-684.

[14] N. Merry, B. Rubinsky, Energy storage in a fluidized bed, J. Heat Transf.-Trans. ASME 111 (1989) 726-730.

[15] R. Brown, J. Rasberry, S. Overmann, Microencapsulated phase-change materials as heat transfer media in gas fluidized beds, Powder Technol. 98 (1998) 217-222.

[16] M. Rady, Study of phase changing characteristics of granular composites using differential scanning calorimetry, Energy Conv. Manag. 29 (2009) 3149-3159.

[17] D. Geldart, Types of gas fluidization. Powder Technol. 7 (1973) 285-292.

[18] D. Kunii, O. Levenspiel, Fluidization Engineering, Butterworth-Heinemann, 2009.

[19] D. Kathuria, S. Saxena, A variable thickness two-dimensional bed for investigating gas-solid fluidized bed hydrodynamics, Powder Technol. 53, (1987) 91-96.

[20] D. Geldart, Gas Fluidization Technology, John Wiley & Sons, 1986.

[21] A. Rees, J. Davidson, J. Dennis, P. Fennell, L. Gladden, A. Hayhurst, M. Mantle, C. Mùller, A. Sederman, The nature of the flow just above the perforated plate distributor of a gas-fluidised bed, as imaged using magnetic resonance, Chem. Eng. Sci. 61 (2006) 6002-6015.

[22] B. Dhifaoui, S. Ben Jabrallah, A. Belghith, J.P. Corriou, Experimental study of the dynamic behaviour of a porous medium submitted to a wall heat flux in view of htermal energy storage by sensible heat, Int. J. Therm. Sci. 46 (2007) 1056-1063.

[23] M. Delgado, A. Lázaro, J. Mazo, B. Zalba, Review of phase change materials emulsions and microencapsulated phase change material slurries: materials, heat transfer studies and applications, Renew. Sust. Energ. Rev. 16 (2012) 253-273.

[24] J. Giro-Paloma, G. Oncins, C. Barreneche, M. Martínez, I. Fernández, L.F. Cabeza, Physico-chemical and mechanical properties of microencapsulated phase change material, Appl. Energ. (2012) http://dx.doi.org/10.1016/j.apenergy.2012.11.007.

[25] R. Yang R, H. Xu, Y. Zhang, Preparation, physical property and thermal physical property of phase change microcapsule slurry and phase change emulsion, Sol. Energ. Mat. Sol. C. 80 (2003) 405-416.

[26] J. Werther, J. Reppenhagen, Attrition, in W.C. Yang (Ed.), Handbook of fluidization and fluid-particle systems, Marcel Dekker Inc., New York, chapter 8.

[27] Y.C. Ray, T.S. Jiang, Particle attrition phenomena in a fluidized bed, Powder Technol. 49 (1987) 193-206.

[28] J.J. Pis, A.B. Fuertes, V. Artos, A. Suárez, F. Rubiera, Attrition of coal ash particles in a fluidized bed, Powder Technol. 66 (1991) 41-46.

List of Figures

1 Schematic representation of the experimental apparatus in mm. 30
2 Variation of the specific heat with temperature for each material. 31
3 Pressure drop across the distributor plate. 32
4 Pressure across the bed at different superficial gas velocities for the sand and the finer GR50. 33
5 Temperature profiles for the sand and the GR50 PCM in fixed and fluidized beds. 34
6 Evolution of efficiency with time for the sand and the GR50 PCM in fixed and fluidized beds during the charging process. 35
7 Evolution of recovery efficiency over time for the sand and the GR50 PCM in fixed and fluidized beds during the discharging periods. 36
8 Temperature profiles for the fluidized bed with GR50 for different flow rates. 37
9 (a) Non-dimensional temperature profiles for the charging of GR50 at different flow rates. (b) Evolution of efficiency over time for the charging of GR50 at different flow rates. 38
10 (a) Non-dimensional temperature profiles for the discharging process of GR50 at different flow rates. (b) Evolution of efficiency over time for the discharging process of GR50 at different flow rates. 39
11 Temperature profiles for the fluidized bed with GR50 for different bed heights. 40
12 (a) Non-dimensional temperature profiles for the charging process of GR50 for different bed heights. (b) Evolution of efficiency with time for the charging process of GR50. 41
13 (a) Non-dimensional temperature profiles for the discharging process of the GR50 for different bed heights. (b) Evolution of efficiency with time for the discharging process of GR50 for different bed heights. 42
14 Temperature profiles for different cycles (under the same conditions) for the PCM in a fluidized bed. 43
15 Cumulative distribution function showing the weight percent of particles passing through a sieve of a given aperture at the beginning, middle and end of the cycling tests. 44

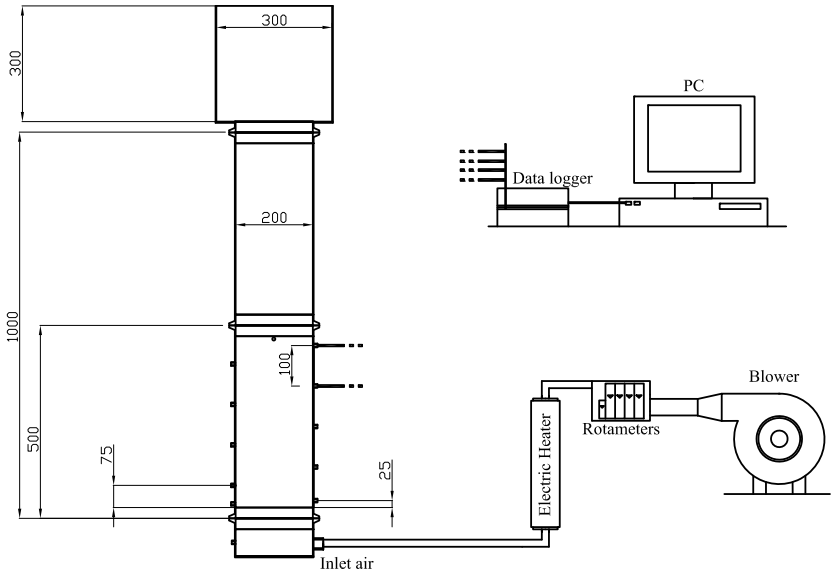

Figure 1: Schematic representation of the experimental apparatus in mm.

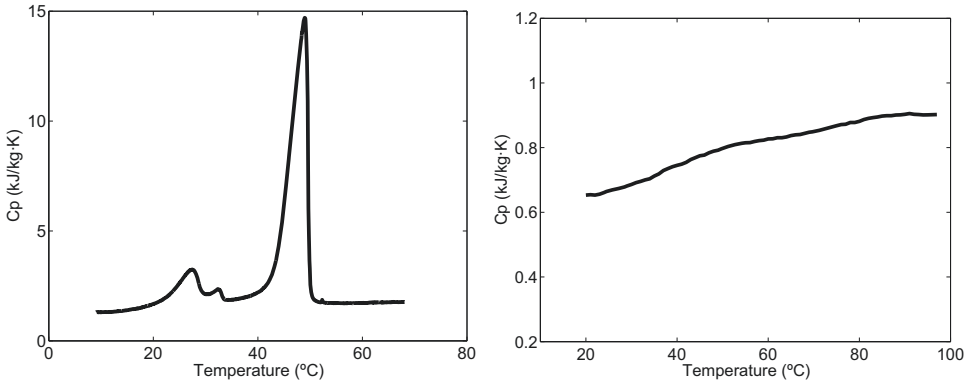

(a) (b)

Figure 2: Variation of the specific heat with temperature for each material.

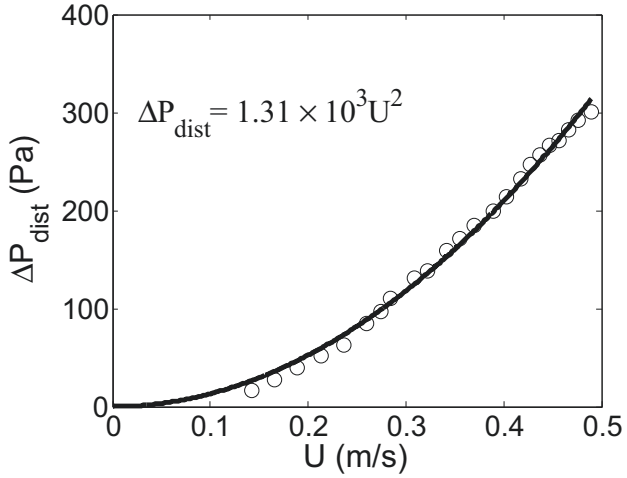

Figure 3: Pressure drop across the distributor plate.

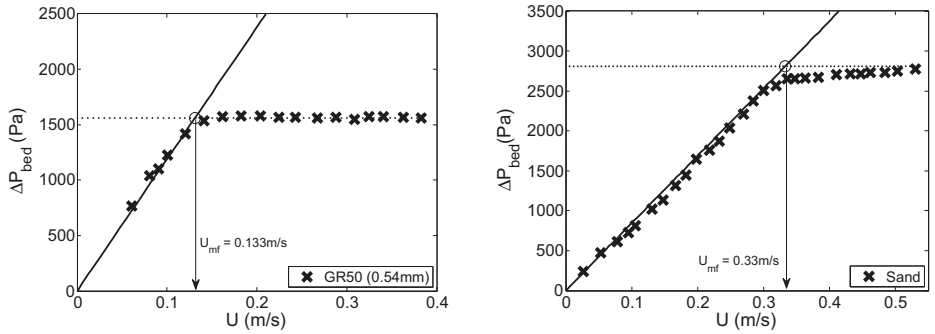

(a) GR50 (b) Sand

Figure 4: Pressure across the bed at different superficial gas velocities for the sand and the finer GR50.

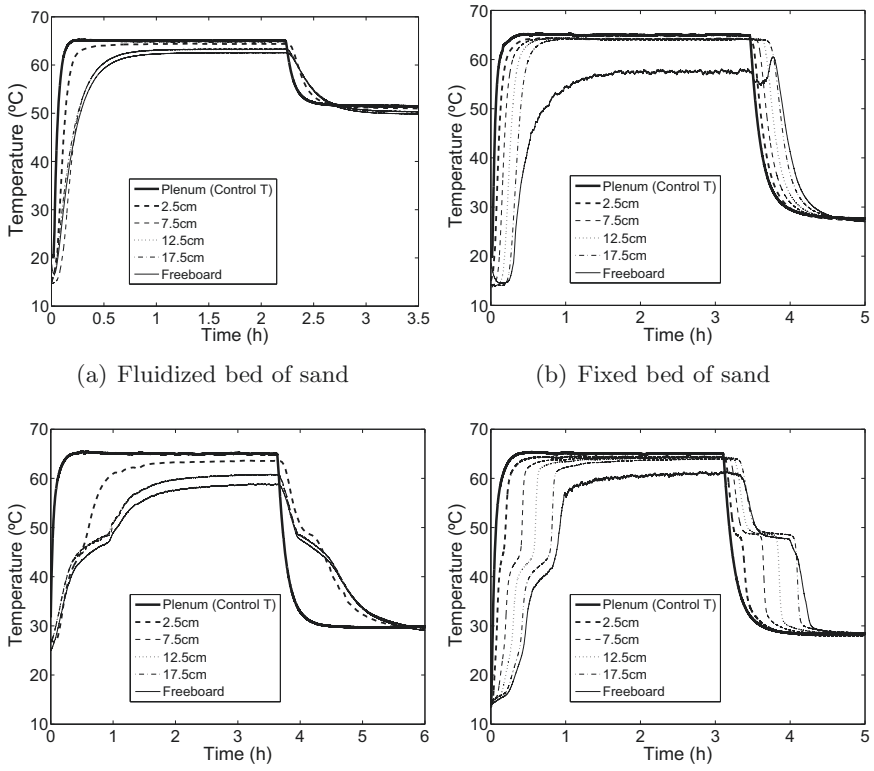

(a) Fluidized bed of sand

(b) Fixed bed of sand

(c) Fluidized bed of GR50 0.54mm

(d) Fixed bed of GR50 1.64mm

Figure 5: Temperature profiles for the sand and the GR50 PCM in fixed and fluidized beds.

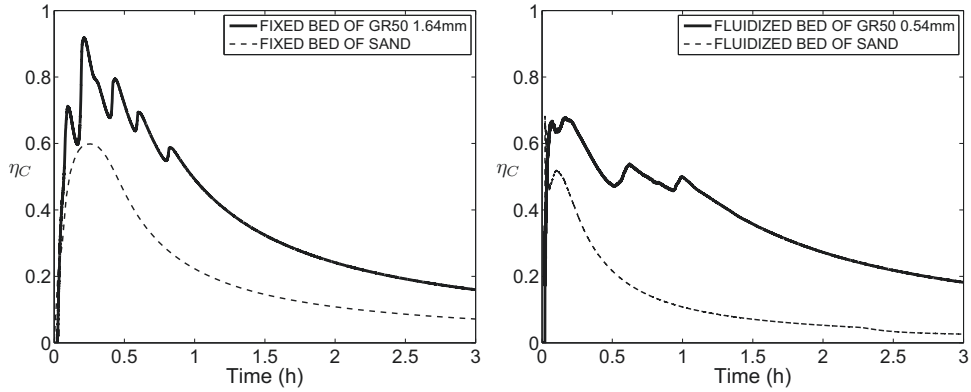

(a) Fixed beds (b) Fluidized beds

Figure 6: Evolution of efficiency with time for the sand and the GR50 PCM in fixed and fluidized beds during the charging process.

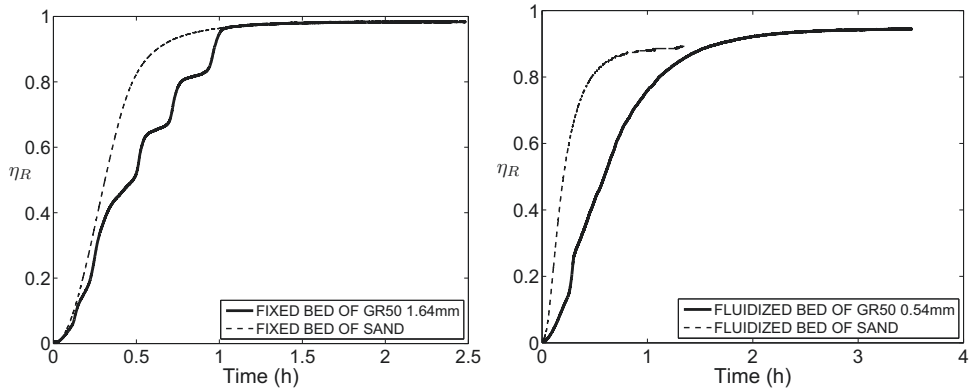

(a) Fixed beds (b) Fluidized beds

Figure 7: Evolution of recovery efficiency over time for the sand and the GR50 PCM in fixed and fluidized beds during the discharging periods.

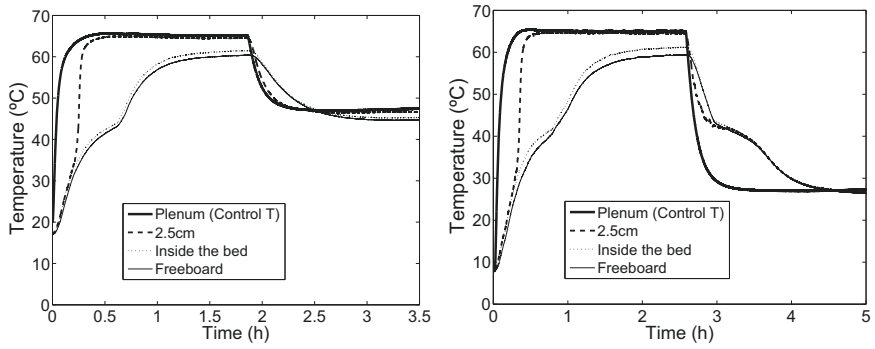

(a) $U = 2.5U_{mf}$

(b) $U = 2U_{mf}$

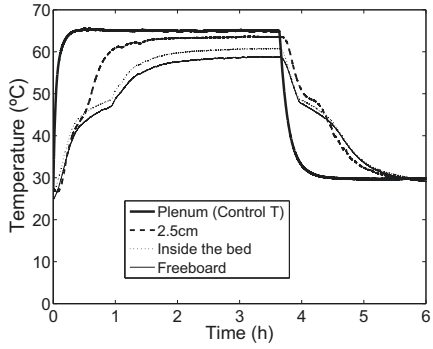

(c) $U = 1.7U_{mf}$

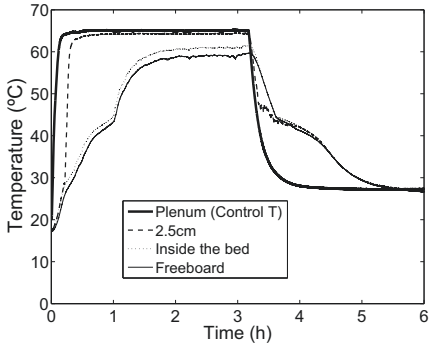

(d) $U = 1.5U_{mf}$

Figure 8: Temperature profiles for the fluidized bed with GR50 for different flow rates.

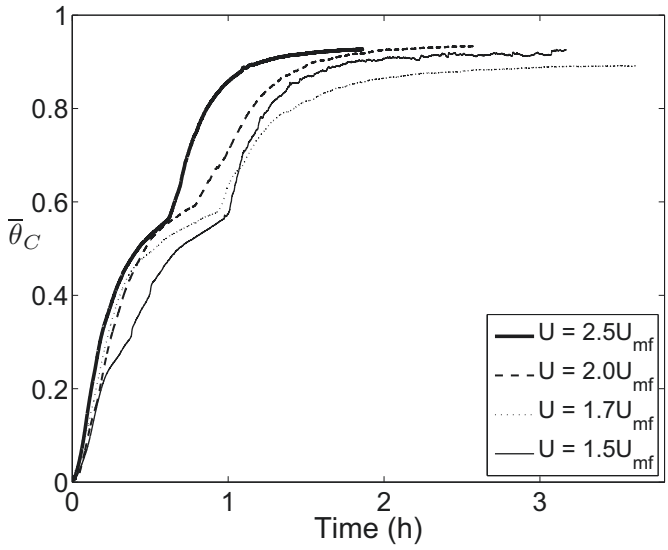

(a)

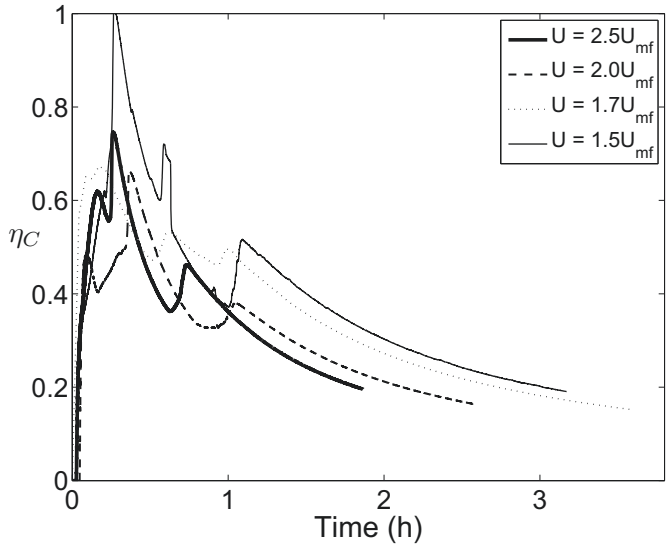

(b)

Figure 9: (a) Non-dimensional temperature profiles for the charging of GR50 at different flow rates. (b) Evolution of efficiency over time for the charging of GR50 at different flow rates.

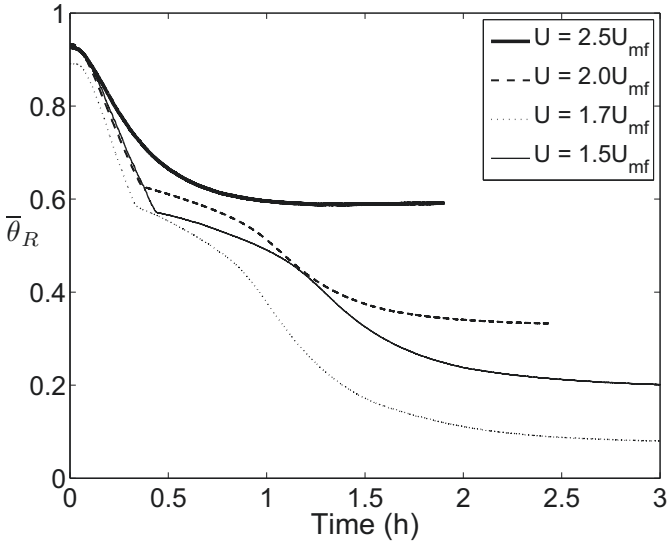

(a)

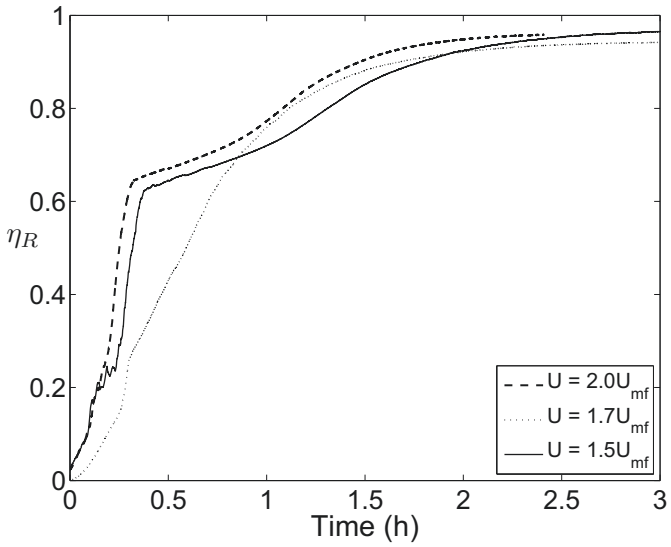

(b)

Figure 10: (a) Non-dimensional temperature profiles for the discharging process of GR50 at different flow rates. (b) Evolution of efficiency over time for the discharging process of GR50 at different flow rates.

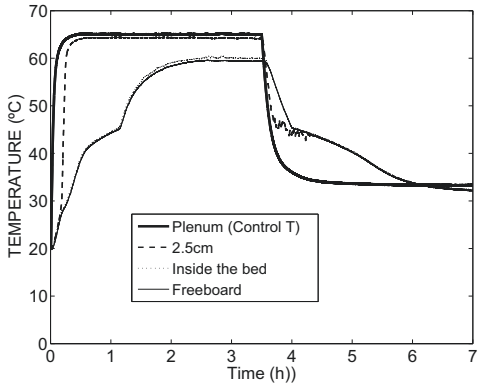

(a) H = 1.5D

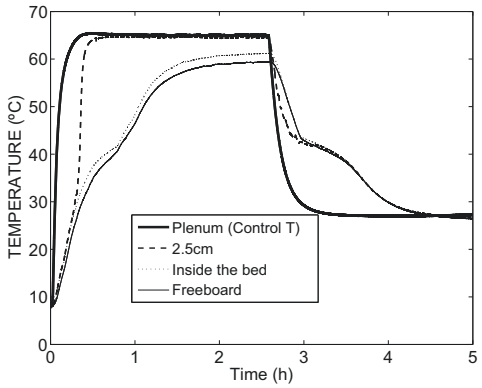

(b) H = 1D

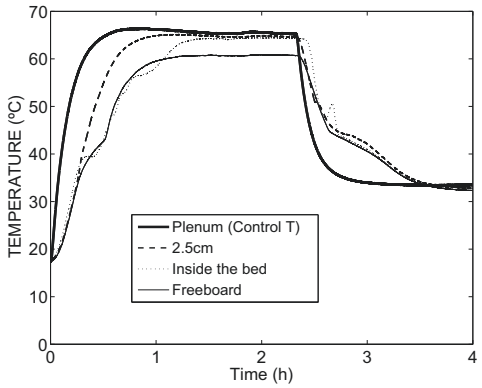

(c) H= 0.5D

Figure 11: Temperature profiles for the fluidized bed with GR50 for different bed heights.

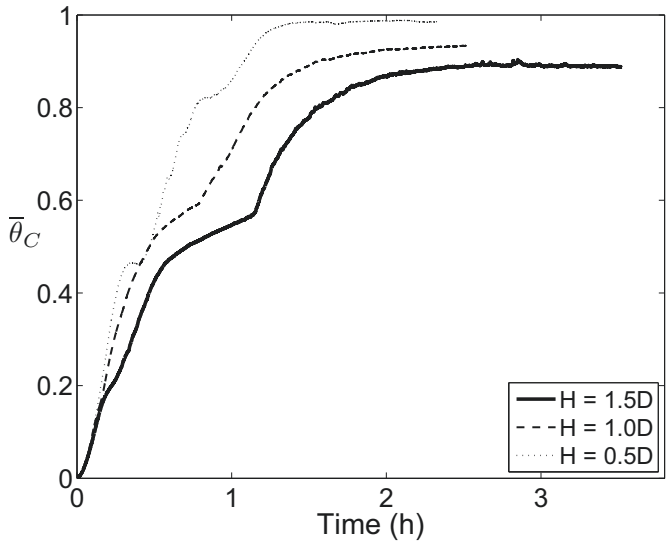

(a)

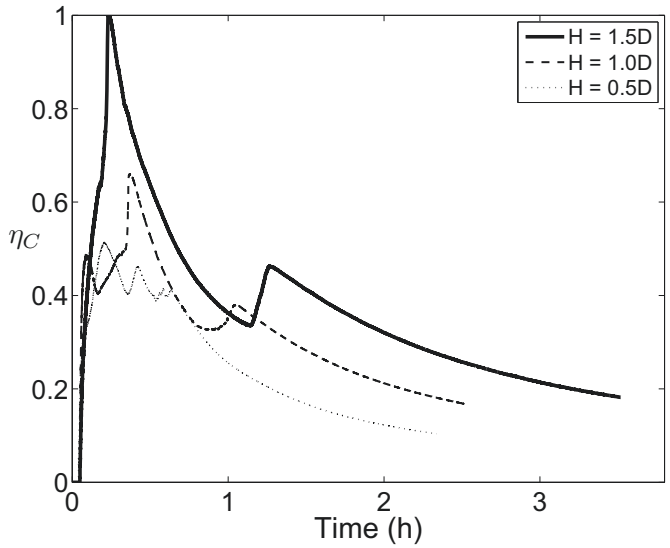

(b)

Figure 12: (a) Non-dimensional temperature profiles for the charging process of GR50 for different bed heights. (b) Evolution of efficiency with time for the charging process of GR50.

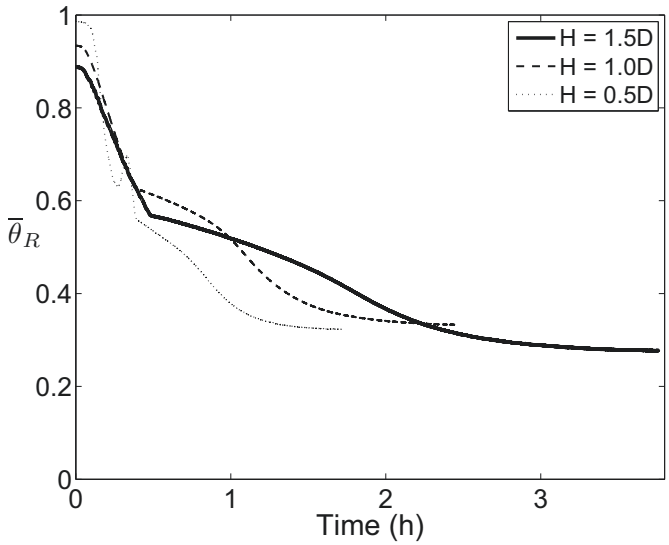

(a)

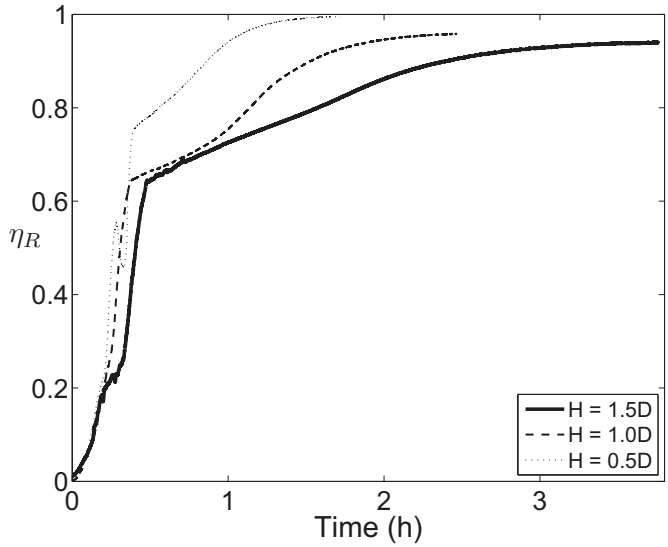

(b)

Figure 13: (a) Non-dimensional temperature profiles for the discharging process of the GR50 for different bed heights. (b) Evolution of efficiency with time for the discharging process of GR50 for different bed heights.

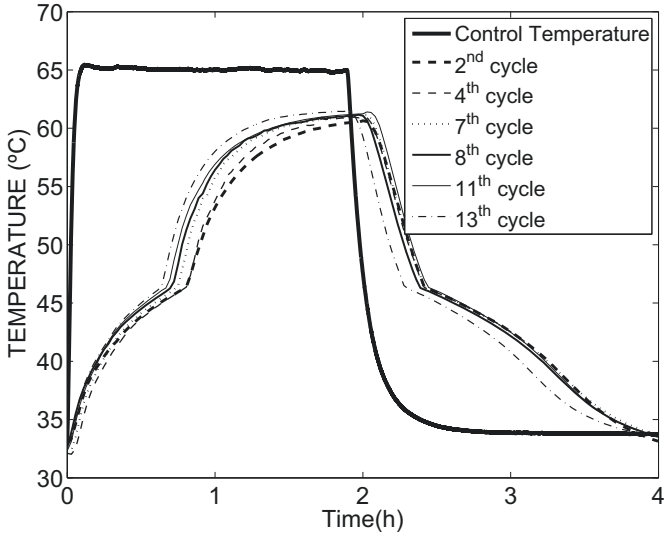

Figure 14: Temperature profiles for different cycles (under the same conditions) for the PCM in a fluidized bed.

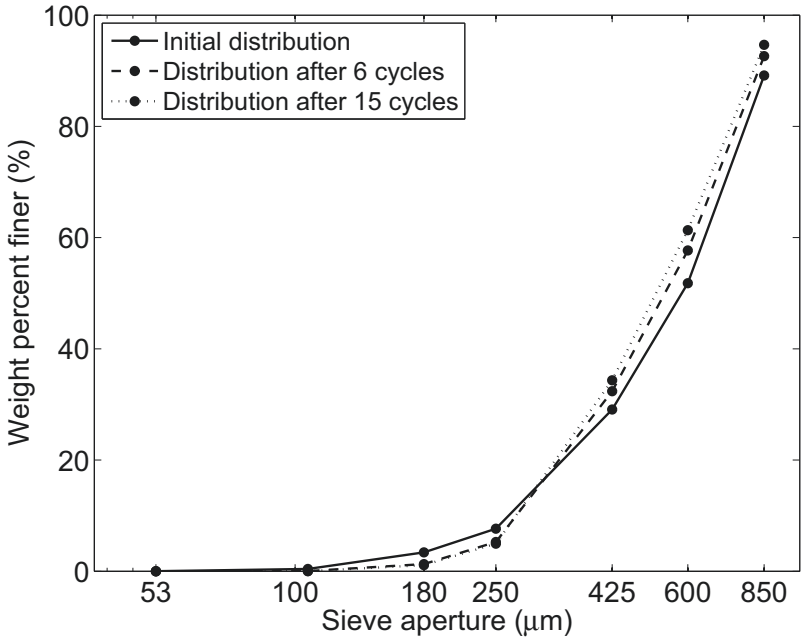

Figure 15: Cumulative distribution function showing the weight percent of particles passing through a sieve of a given aperture at the beginning, middle and end of the cycling tests.

List of Tables

1 Properties of the materials used in these experiments. [1]Measured at room temperature. [2]Data from the manufacturer. 46
2 Characterization of the PCM using DSC. 47

Material	ρ [kg/m^3][1]	k [W/mK][2]	$\overline{d_p}$ [mm][1]	σ_{dp} [mm][1]
Sand	2632.3	0.27	0.6	
Finer GR50	1550.5	0.2	0.54	0.082
Coarser GR50	1512.8	0.2	1.64	0.196

Table 1: Properties of the materials used in these experiments. [1]Measured at room temperature. [2]Data from the manufacturer.

Material	$c_{p,s}[J/kgK]$	$c_{p,l}[J/kgK]$	$h_{ls}[J/kg]$	$T_{on}[^\circ C]$	$T_s[^\circ C]$	$T_e[^\circ C]$	$T_{end}[^\circ C]$	$T_p[^\circ C]$
Finer GR50	1458.3	1668.7	52049.8	39.4	45.3	51.6	54.3	49.8
Coarser GR50	1448.6	1735.7	54379	38.6	45.3	51.8	56.2	50

Table 2: Characterization of the PCM using DSC.